



Cite this: *New J. Chem.*, 2024, 48, 8093

Adsorption of gases on B₁₂N₁₂ and Al₁₂N₁₂ nanocages†

Remya Geetha Sadasivan Nair, * Arun Kumar Narayanan Nair * and Shuyu Sun*

Density functional theory (DFT) was used to investigate the adsorption of twenty-four gases (SiH₄, H₂, Cl₂, F₂, CF₄, CH₄, CF₂Cl₂, N₂, CHF₃, OCS, N₂O, AsH₃, CH₃Cl, COCl₂, C₂H₂, C₂H₄, H₂Se, H₂S, PH₃, COF₂, CH₃F, HCHO, (CH₃)₂O, and CH₃NH₂) on B₁₂N₁₂ and Al₁₂N₁₂ nanocages. Most of the studied gases are weakly (strongly) adsorbed on the B₁₂N₁₂ (Al₁₂N₁₂) nanocage. However, AsH₃, H₂Se, H₂S, PH₃, CH₃F, HCHO, (CH₃)₂O, and CH₃NH₂ are strongly adsorbed on the B₁₂N₁₂ nanocage and H₂, F₂, CF₄, CH₄, and CF₂Cl₂ are weakly adsorbed on the Al₁₂N₁₂ nanocage. The most negative-valued molecular electrostatic potential (MESP) minimum (*V*_{min}) corresponds to the electron-rich region (e.g., lone pair and π -bond) in the molecule. An important observation is that the adsorption energies of the gases on the B₁₂N₁₂ and Al₁₂N₁₂ nanocages are well correlated with the MESP *V*_{min} values of the gases. Substantial changes are found in the DFT reactivity indices like chemical potential and hardness of the B₁₂N₁₂ and Al₁₂N₁₂ nanocages, mainly due to the strong gas adsorption. The quantum theory of atoms in molecules analysis suggests the covalent nature of interactions only in the AsH₃/B₁₂N₁₂, H₂Se/B₁₂N₁₂, H₂S/B₁₂N₁₂, and PH₃/B₁₂N₁₂ systems.

Received 12th December 2023,
Accepted 29th March 2024

DOI: 10.1039/d3nj05703h

rsc.li/njc

1. Introduction

Air pollution due to rapid urbanization and economic developments is a major environmental concern. Methane (CH₄) and nitrous oxide (N₂O) are the most important anthropogenic contributors to the greenhouse effect after carbon dioxide (CO₂).^{1,2} Enteric fermentation and the oil and gas industry have been identified as the two main sources of anthropogenic CH₄. The use of nitrogen fertilizers is identified as an important source of nitrous oxide (N₂O) emissions. Hydrogen sulfide (H₂S) is a highly toxic gas released from sewage treatment processes, fuel burning, and petroleum extraction.³ Carbonyl sulfide (OCS) is released from the burning of biomass and fossil fuel, as well as petrochemical and gasification processes.⁴ Halomethanes are found both in marine environments and those of man-made origin, and some of them are widespread and hazardous.^{5,6} For example, the ultraviolet photolysis of refrigerants such as dichlorodifluoromethane (CF₂Cl₂) can damage the stratospheric ozone layer. Silane (SiH₄) finds applications in the photovoltaic and semiconductor industries.⁷ Hydrogen selenide (H₂Se) is used in the preparation of materials for battery applications.⁸ Chlorine (Cl₂) can be used for the

sterilization of drinking water.⁹ Fluorine (F₂) plays a key role in the pharmaceutical industry.¹⁰ The pnictogen hydride gases phosphine (PH₃)¹¹ and arsine (AsH₃)¹² are used as a fumigant and in the semiconductor industry, respectively. Phosgene (COCl₂) is of historical interest (chemical weapon in World War I) and currently used in the manufacture of polyurethanes, polycarbonates, dyestuff, pharmaceuticals, *etc.*¹³ The usage of carbonyl fluoride (COF₂) as a cleaning gas could reduce the greenhouse gas emissions from the semiconductor industry.¹⁴ Formaldehyde (HCHO) is mainly used to synthesize resins.¹⁵ Dimethyl ether ((CH₃)₂O) can be used as an aerosol propellant and as an alternative to diesel fuel.¹⁶ Methylamine (CH₃NH₂) is used for fabricating perovskite solar cells.¹⁷ However, these gases could cause severe health and safety concerns. Hydrogen (H₂) storage is a key issue in developing materials which could be utilized for fuel cell technology.¹⁸ Nitrogen (N₂) is often used in modeling the adsorption process.¹⁹ There are growing interests in gas capture and storage necessitated by concerns arising from the demand to mitigate air pollution. Materials like metal-organic framework, zeolite, graphene, fullerene, carbon nanotube, polymer, clay, cyclo[*n*]carbon, *etc.* exhibit promising potential for applications in gas capture and storage.^{20–27}

There have been density functional theory (DFT) studies of the gas-adsorption on nanoparticles and nanosheets. Abbasi *et al.* found that the adsorption of NO₂, CH₂O and H₂S molecules on the N-doped TiO₂ anatase nanoparticles is energetically more favorable than the adsorption on the pristine ones.^{28–30} The adsorption behaviors of SO_x molecules showed

Physical Science and Engineering Division (PSE), Computational Transport Phenomena Laboratory, King Abdullah University of Science and Technology (KAUST), Thuwal 23955-6900, Saudi Arabia. E-mail: remya.nair@kaust.edu.sa, arun.narayanan@kaust.edu.sa, shuyu.sun@kaust.edu.sa

† Electronic supplementary information (ESI) available: Additional details of DFT analysis. See DOI: <https://doi.org/10.1039/d3nj05703h>



an improved adsorption ability for N-doped ZnO nanoparticles over undoped nanoparticles.³¹ The interaction of O₃ and NO₂ with the N-doped TiO₂/ZnO nanocomposite was stronger than with the pristine one.³² The noble metal (Rh, Pt, Pd) decorated N-doped graphene may potentially be used as sensors for biogas detection.³³ The B-doped stanene may be a good candidate for gas sensing.^{34,35} It was found that the O₃, SO₂, and SO₃ molecules weakly interact with the MoS₂ monolayer.³⁶ The adsorption of CO and NO molecules on the doped MoS₂ monolayers was more favorable in energy than that on the pristine monolayers.³⁷

The gas-adsorption on fullerene-like B₁₂N₁₂ and Al₁₂N₁₂ nanocages has attracted a lot of interest in recent years.^{27,38–51} The synthesis of the fullerene-like B₁₂N₁₂ nanocage clusters has been reported.⁵² There have been reports of the synthesis of AlN nanotube and nanocone.^{53,54} The Al₁₂N₁₂ nanocage has been computed to be the most stable of the Al_nN_n ($n = 2–41$) nanocages.⁵⁵ The DFT studies showed that the adsorption of CH₄ has no significant effect on the electronic properties of the B₁₂N₁₂ nanocage.³⁸ H₂S showed a weak physisorption on the B₁₂N₁₂ nanocage.³⁹ The formaldehyde adsorption induced considerable variation in the electronic properties of the B₁₂N₁₂ nanocage.⁴⁰ The adsorption of N₂ and F₂ showed negligible changes on the electronic and structural properties of the B₁₂N₁₂ nanocage.⁴¹ Higher values of adsorption energy were obtained for CH₃F than for CH₃Cl on the B₁₂N₁₂ nanocage.⁴² NH₃ molecule was adsorbed on the B₁₂N₁₂ nanocage with considerable adsorption energy, while the PH₃ and AsH₃ molecules were relatively weakly adsorbed.⁴³ DFT studies showed that CH₃Cl and CH₃F strongly interact with the Al₁₂N₁₂ nanocage.⁴⁴ It was found that H₂S and OCS strongly interact with the Al₁₂N₁₂ nanocage.⁴⁵ Acetylene and ethylene interact preferably with an Al atom rather than N atom of the Al₁₂N₁₂ nanocage.⁴⁶ A very weak adsorption of H₂ on the B₁₂N₁₂ and Al₁₂N₁₂ nanocages has been reported.^{47–49} It was found that dimethyl ether chemisorbed on the B₁₂N₁₂ and Al₁₂N₁₂ nanocages.⁵⁰ The adsorption of phosgene molecules on the B₁₂N₁₂ (Al₁₂N₁₂) nanocage

proceeds by way of physisorption (chemisorption).⁵¹ We recently investigated the adsorption process of NO, CO₂, CO, and NH₃ on the B₁₂N₁₂ and Al₁₂N₁₂ nanocages using DFT calculations.²⁷ It was found that, for example, NH₃ chemisorbed on the B₁₂N₁₂ and Al₁₂N₁₂ nanocages.²⁷ However, adsorption of gases like SiH₄ on the B₁₂N₁₂ and Al₁₂N₁₂ nanocages has yet to be studied.

In this study, we perform DFT calculations to understand the adsorption behavior of SiH₄, H₂, Cl₂, F₂, CF₄, CH₄, CF₂Cl₂, N₂, CHF₃, OCS, N₂O, AsH₃, CH₃Cl, COCl₂, C₂H₂, C₂H₄, H₂Se, H₂S, PH₃, COF₂, CH₃F, HCHO, (CH₃)₂O, and CH₃NH₂ on the B₁₂N₁₂ and Al₁₂N₁₂ nanocages. Most of the studied gases are weakly (strongly) adsorbed on the B₁₂N₁₂ (Al₁₂N₁₂) nanocage. The most negative-valued molecular electrostatic potential (MESP) minimum (V_{\min}) corresponds to the electron-rich region (e.g., lone pair and π -bond) in the molecule.^{56–58} An important observation is that the adsorption energies of the gases on the B₁₂N₁₂ and Al₁₂N₁₂ nanocages are well correlated with the MESP V_{\min} values of the gases. Our results are expected to contribute to the exploration and development of promising adsorbents for gas capture and sequestration.

2. Computational details and calculations

We recently studied the adsorption of NO, CO₂, CO, and NH₃ on B₁₂N₁₂ and Al₁₂N₁₂ nanocages using DFT calculations.²⁷ Here we study the adsorption of an additional 24 gases (SiH₄, H₂, Cl₂, F₂, CF₄, CH₄, CF₂Cl₂, N₂, CHF₃, OCS, N₂O, AsH₃, CH₃Cl, COCl₂, C₂H₂, C₂H₄, H₂Se, H₂S, PH₃, COF₂, CH₃F, HCHO, (CH₃)₂O, and CH₃NH₂) on B₁₂N₁₂ and Al₁₂N₁₂ nanocages using DFT calculations. All the DFT calculations were performed with the Gaussian 16 code.⁵⁹ All structures were optimized at the M062X/6-311G(d,p) level.⁶⁰ The harmonic frequencies (all positive) were computed to confirm the minimal nature of the optimized structures. The MESP topographical analysis of molecules were

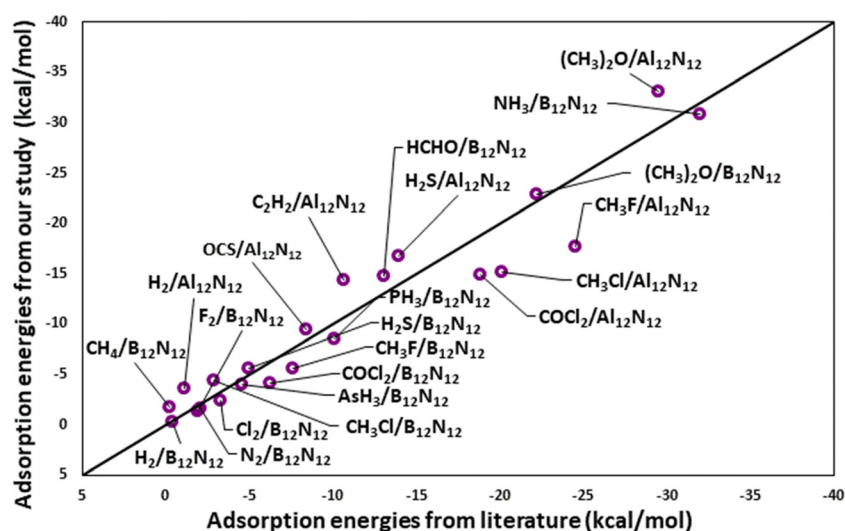


Fig. 1 Comparison of our results for adsorption energies with literature values.^{38–51}



performed at the M062X/6-311G(d,p) level. The MESP, $V(\mathbf{r})$, is expressed as^{56–58}

$$V(\mathbf{r}) = \sum_{A=1}^N \frac{Z_A}{|\mathbf{r} - \mathbf{R}_A|} - \int \frac{\rho(\mathbf{r}')}{|\mathbf{r} - \mathbf{r}'|} d^3\mathbf{r}' \quad (1)$$

where Z_A and $\rho(\mathbf{r})$ represent charge on nucleus A located at \mathbf{R}_A and electronic charge density, respectively. The first and second terms in eqn (1) stand for the nuclear and electronic contributions, respectively. The sign of $V(\mathbf{r})$ is positive when the first term in eqn (1) is dominant and negative when the second term in eqn (1) is dominant.

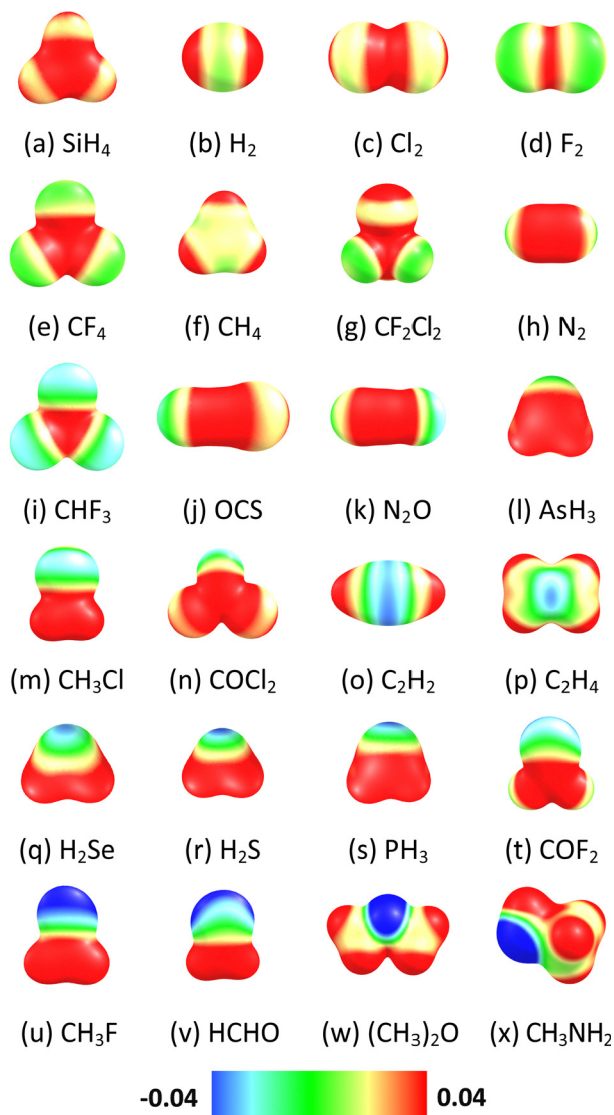


Fig. 2 MESP mapped onto the 0.01 a.u. electron density isosurface of (a) SiH₄, (b) H₂, (c) Cl₂, (d) F₂, (e) CF₄, (f) CH₄, (g) CF₂Cl₂, (h) N₂, (i) CHF₃, (j) OCS, (k) N₂O, (l) AsH₃, (m) CH₃Cl, (n) COCl₂, (o) C₂H₂, (p) C₂H₄, (q) H₂Se, (r) H₂S, (s) PH₃, (t) COF₂, (u) CH₃F, (v) HCHO, (w) (CH₃)₂O, and (x) CH₃NH₂. Color code: blue –0.04 a.u. to red 0.04 a.u. Blue represents the most electron-rich region and red the most electron-poor region.

The DFT reactivity indices are given by^{61–66}

$$\text{Electronic chemical potential, } \mu = \frac{E_{\text{LUMO}} + E_{\text{HOMO}}}{2} \quad (2)$$

$$\text{Chemical hardness, } \eta = \frac{E_{\text{LUMO}} - E_{\text{HOMO}}}{2} \quad (3)$$

$$\text{Global softness, } S = \frac{1}{2\eta} \quad (4)$$

$$\text{Global electrophilicity, } \omega = \frac{\mu^2}{2\eta} \quad (5)$$

where E_{HOMO} and E_{LUMO} denote the energy of the highest occupied molecular orbital (HOMO) and the lowest unoccupied molecular orbital (LUMO), respectively. These DFT reactivity indices may give insight into the chemical reactivities.

The adsorption energy (E_{ads}) is given by

$$E_{\text{ads}} = E_{\text{gas/nanocage}} - (E_{\text{nanocage}} + E_{\text{gas}}) \quad (6)$$

where $E_{\text{gas/nanocage}}$, E_{nanocage} , and E_{gas} represent the energy of gas-adsorbed nanocage, nanocage (e.g., B₁₂N₁₂), and gas (e.g., SiH₄), respectively.

The adsorption free energy (G_{ads}) is given by

$$G_{\text{ads}} = G_{\text{gas/nanocage}} - (G_{\text{nanocage}} + G_{\text{gas}}) \quad (7)$$

where $G_{\text{gas/nanocage}}$, G_{nanocage} , and G_{gas} represent the free energy of gas-adsorbed nanocage, nanocage, and gas respectively. The adsorption energies and free energies were corrected for the basis set superposition errors with the counterpoise method.⁶⁷ It may be noted that our E_{ads} values are consistent with earlier works^{38–51} (Fig. 1).

Furthermore, Bader's quantum theory of atoms in molecules (QTAIM) analysis⁶⁸ at the M062X/6-311G(d,p) level was performed using Multiwfn software.⁶⁹ The covalent and noncovalent bonding scenario can be analyzed based on the value of ρ and its Laplacian ($\nabla^2\rho$) at the bond critical point. Usually, for the covalent interaction, ρ is relatively high and $\nabla^2\rho < 0$, while for the non-covalent interaction (van der Waals, ionic, etc.), ρ is relatively low and $\nabla^2\rho > 0$.^{70,71} The electron localization function (ELF)⁷² and localized orbital locator (LOL)⁷³ were calculated

Table 1 MESP $V_{\text{min-x}}$ for adsorbate gases. Values in kcal mol^{–1}

Adsorbate	$V_{\text{min-x}}$	Adsorbate	$V_{\text{min-x}}$
SiH ₄	–0.94	AsH ₃	–15.88
H ₂	–2.64	CH ₃ Cl	–17.07
Cl ₂	–2.76	COCl ₂	–20.65
F ₂	–2.76	C ₂ H ₂	–21.15
CF ₄	–2.95	C ₂ H ₄	–21.27
CH ₄	–3.07	H ₂ Se	–21.77
CF ₂ Cl ₂	–3.89	H ₂ S	–23.78
NO ^a	–8.97	PH ₃	–23.91
N ₂	–11.92	COF ₂	–24.85
CHF ₃	–12.86	CH ₃ F	–31.31
OCS	–14.12	HCHO	–41.92
CO ₂ ^a	–14.87	(CH ₃) ₂ O	–52.02
N ₂ O	–15.19	NH ₃ ^a	–73.23
CO ^a	–15.88	CH ₃ NH ₂	–75.80

^a Taken from ref. 27.



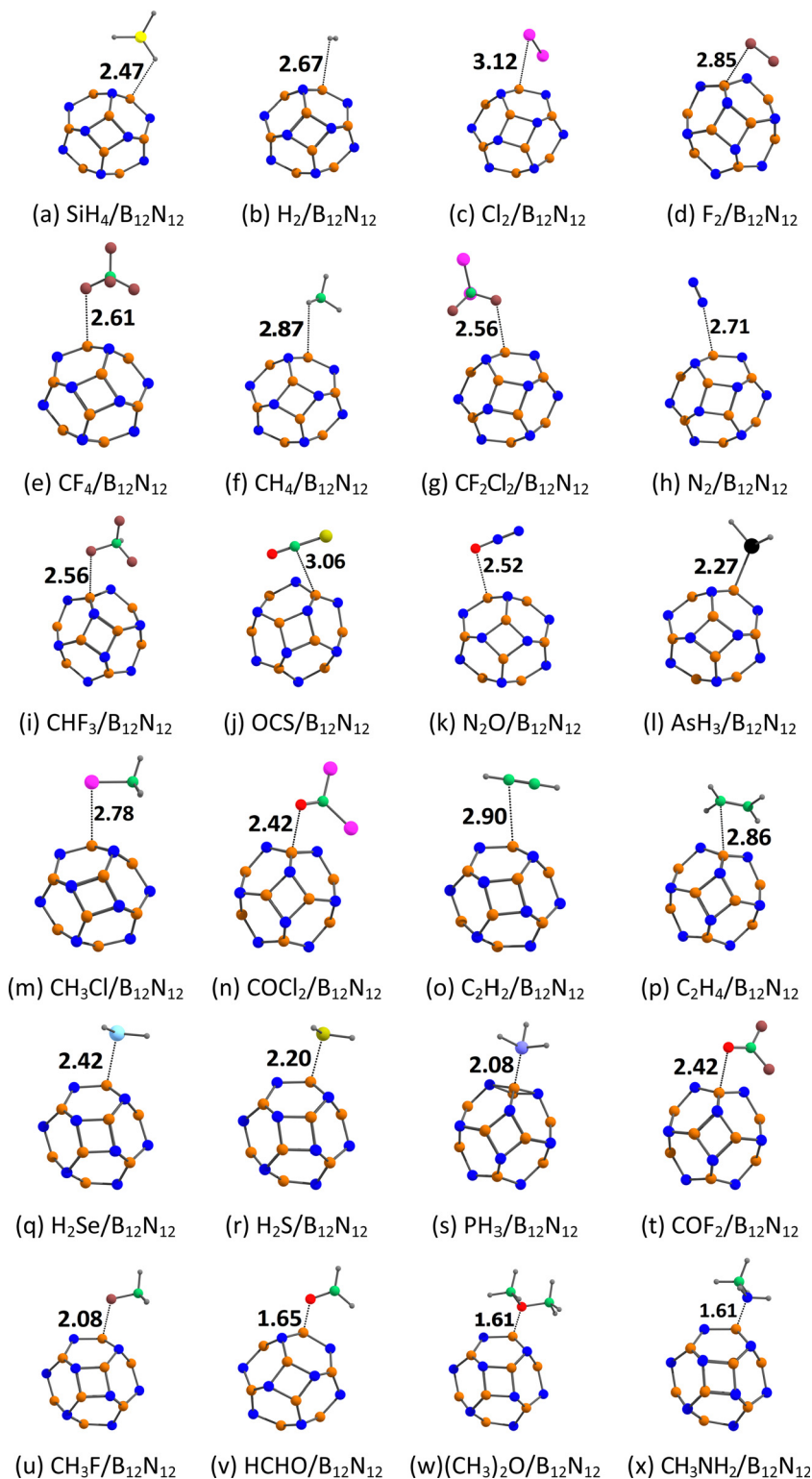


Fig. 3 Optimized structures of gases (a) SiH_4 , (b) H_2 , (c) Cl_2 , (d) F_2 , (e) CF_4 , (f) CH_4 , (g) CF_2Cl_2 , (h) N_2 , (i) CHF_3 , (j) OCS , (k) N_2O , (l) AsH_3 , (m) CH_3Cl , (n) COCl_2 , (o) C_2H_2 , (p) C_2H_4 , (q) H_2Se , (r) H_2S , (s) PH_3 , (t) COF_2 , (u) CH_3F , (v) HCHO , (w) $(\text{CH}_3)_2\text{O}$, and (x) CH_3NH_2 adsorbed on $\text{B}_{12}\text{N}_{12}$. The adsorption distances are given in Å. Color code: green-C, orange-B, blue-N, yellow-Si, gray-H, pink-Cl, brown-F, red-O, cyan-Se, yellowish green-S, black-As, violet-P.

using the Multiwfn program.⁶⁹ The relatively high values of ELF and LOL are indicative of covalent interactions. The non-covalent interaction (NCI) analysis^{74,75} was performed

using the Multiwfn program⁶⁹ and the results were visualized with the GnuPlot⁷⁶ and visual molecular dynamics (VMD) software.⁷⁷



Table 2 Adsorption distance, E_{ads} , G_{ads} , MESP V_{min} , and ΔV_{min} for the gas-adsorbed $\text{B}_{12}\text{N}_{12}$ nanocage. d_{ads} is given in Å, other values are given in kcal mol $^{-1}$

Adsorbate	d_{ads}	E_{ads}	G_{ads}	$V_{\text{min-C'}}$	$\Delta V_{\text{min-C}}$
SiH_4	2.47	-2.47	5.86	-21.77	-1.00
H_2	2.67	-0.83	3.94	-21.34	-0.56
Cl_2	3.12	-2.36	4.84	-21.40	-0.63
F_2	2.85	-1.34	5.65	-21.59	-0.82
CF_4	2.61	-2.08	6.60	-21.90	-1.13
CH_4	2.87	-1.70	3.21	-21.27	-0.50
CF_2Cl_2	2.56	-2.20	7.32	-22.84	-2.07
NO^a	2.54	-2.77	3.46	-22.90	-2.13
N_2	2.71	-1.60	3.27	-22.21	-1.44
CHF_3	2.56	-3.57	5.74	-24.47	-3.70
OCS	3.06	-2.65	4.77	-23.85	-3.07
CO_2^a	2.66	-2.95	3.51	-22.53	-1.76
N_2O	2.52	-3.69	3.88	-24.10	-3.33
CO^a	1.79	-1.65	7.64	-27.92	-7.15
AsH_3	2.27	-4.05	6.27	-30.94	-10.17
CH_3Cl	2.78	-4.45	4.21	-25.04	-4.27
COCl_2	2.42	-4.11	7.00	-26.17	-5.40
C_2H_2	2.90	-3.54	1.64	-24.85	-4.08
C_2H_4	2.86	-3.87	4.04	-23.22	-2.45
H_2Se	2.42	-4.44	3.87	-28.68	-7.91
H_2S	2.20	-5.64	4.45	-29.81	-9.04
PH_3	2.08	-8.49	2.38	-32.82	-12.05
COF_2	2.42	-3.91	5.35	-26.42	-5.65
CH_3F	2.08	-5.64	3.83	-29.87	-9.10
HCHO	1.65	-14.76	-2.16	-33.63	-12.86
$(\text{CH}_3)_2\text{O}$	1.61	-22.86	-9.57	-34.20	-13.43
NH_3^a	1.62	-30.82	-18.62	-34.89	-14.12
CH_3NH_2	1.61	-36.84	-23.22	-35.27	-14.50

^a Taken from ref. 27.

3. Results and discussion

3.1. MESP

The MESP maps of the gas molecules are given in Fig. 2. A visual check of the MESP maps shows the presence of a blue region (most electron-rich region) in, for example, the formaldehyde, dimethyl ether, and methylamine molecules. The blue region is situated close to the O atoms of the formaldehyde and dimethyl ether molecules, and the N atom of the methylamine

molecule. The MESP V_{min} values of the gas molecules (represented as $V_{\text{min-X}}$) are given in Table 1. The locations of the MESP V_{min} for a few representative cases are given in Fig. S1 (ESI †). Here these $V_{\text{min-X}}$ values are in the range of -0.94 (SiH_4) to -75.80 kcal mol $^{-1}$ (CH_3NH_2). The MESP V_{min} values of the diatomic gases follow the order: $\text{H}_2 < \text{Cl}_2 < \text{F}_2 < \text{NO} < \text{N}_2 < \text{CO}$. The MESP V_{min} values of the triatomic molecules follow the order: $\text{OCS} < \text{CO}_2 < \text{N}_2\text{O} < \text{H}_2\text{Se} < \text{H}_2\text{S}$. The MESP V_{min} value of silane is lower than that of methane (-3.07 kcal mol $^{-1}$). The MESP V_{min} values of the hydrocarbon gases follow the order: methane $<$ acetylene $<$ ethylene. The MESP V_{min} values of the halomethanes follow the order: $\text{CF}_4 < \text{CF}_2\text{Cl}_2 < \text{CHF}_3 < \text{CH}_3\text{Cl} < \text{CH}_3\text{F}$. The MESP V_{min} values of formaldehyde and its halogenated derivatives follow the order: phosgene $<$ carbonyl fluoride $<$ formaldehyde. The MESP V_{min} value of dimethyl ether (-52.02 kcal mol $^{-1}$) is lower than that of both ammonia (-73.23 kcal mol $^{-1}$) and methylamine. The MESP V_{min} values of the pnictogen hydrides and methylamine follow the order arsine $<$ phosphine $<$ ammonia $<$ methylamine.

Both of the $\text{B}_{12}\text{N}_{12}$ and $\text{Al}_{12}\text{N}_{12}$ nanocages consist of 6 tetragonal and 8 hexagonal rings 27,78 (Fig. S2, ESI †). These nanocages have two distinct B–N or Al–N bonds. Here, the two hexagonal rings share the shorter B–N (1.44 Å) or Al–N bond (1.78 Å), and the tetragonal and the hexagonal rings share the longer B–N (1.48 Å) or Al–N bond (1.85 Å). A visual check of the MESP maps shows that the blue regions (most electron-rich regions) are situated close to the N atoms of the $\text{B}_{12}\text{N}_{12}$ and $\text{Al}_{12}\text{N}_{12}$ nanocages (see Fig. S2, ESI †). It may be noted that the MESP V_{min} values of $\text{B}_{12}\text{N}_{12}$ and $\text{Al}_{12}\text{N}_{12}$ (represented as $V_{\text{min-C}}$) are -20.77 and -49.07 kcal mol $^{-1}$ respectively. 27

3.2. Adsorption of gases on $\text{B}_{12}\text{N}_{12}$

The optimized structures of the gases adsorbed on the $\text{B}_{12}\text{N}_{12}$ nanocage are given in Fig. 3. The studied gases are preferably bound to the B atom rather than the N atom of the $\text{B}_{12}\text{N}_{12}$ nanocage. Notably, the F atom of the CF_2Cl_2 , the C atom of the

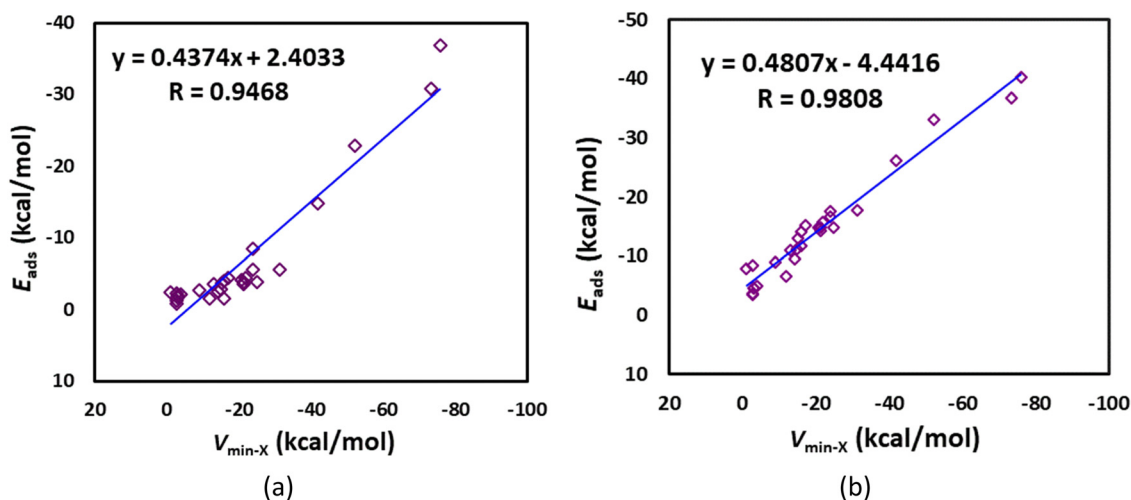


Fig. 4 Correlation between $V_{\text{min-X}}$ and E_{ads} for gas-adsorbed (a) $\text{B}_{12}\text{N}_{12}$ and (b) $\text{Al}_{12}\text{N}_{12}$ nanocages.



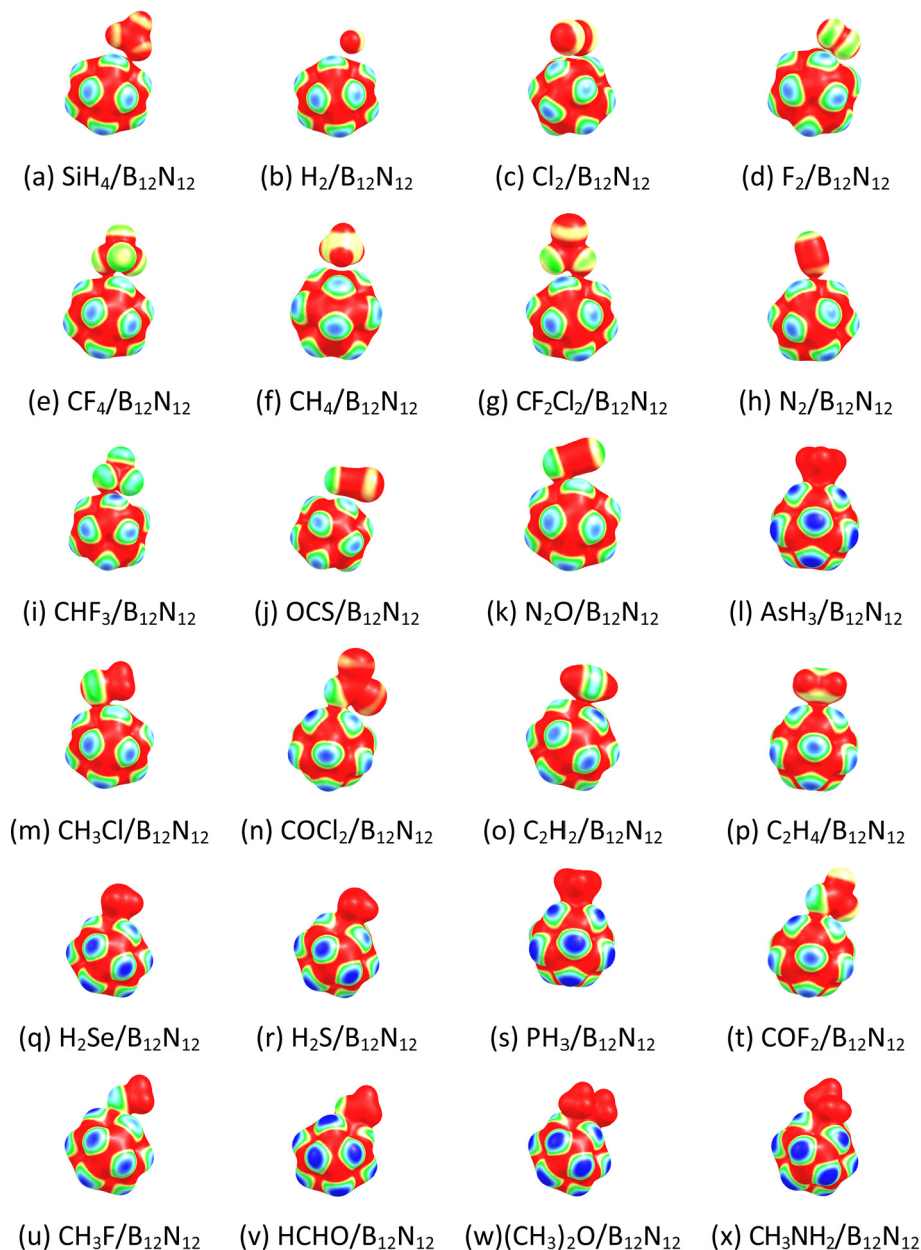


Fig. 5 MESP mapped onto 0.01 a.u. electron density isosurface of gases (a) SiH_4 , (b) H_2 , (c) Cl_2 , (d) F_2 , (e) CF_4 , (f) CH_4 , (g) CF_2Cl_2 , (h) N_2 , (i) CHF_3 , (j) OCS , (k) N_2O , (l) AsH_3 , (m) CH_3Cl , (n) COCl_2 , (o) C_2H_2 , (p) C_2H_4 , (q) H_2Se , (r) H_2S , (s) PH_3 , (t) COF_2 , (u) CH_3F , (v) HCHO , (w) $(\text{CH}_3)_2\text{O}$, and (x) CH_3NH_2 adsorbed on $\text{B}_{12}\text{N}_{12}$. The color code is the same as in Fig. 2.

OCS , and the O atom of the N_2O are bound to the B atom of the $\text{B}_{12}\text{N}_{12}$ nanocage. Typically, the studied gases are weakly adsorbed on the $\text{B}_{12}\text{N}_{12}$ nanocage. However, CO , AsH_3 , H_2Se , H_2S , PH_3 , CH_3F , HCHO , $(\text{CH}_3)_2\text{O}$, NH_3 , and CH_3NH_2 are strongly adsorbed on the $\text{B}_{12}\text{N}_{12}$ nanocage. Typically, the gases strongly interact with the $\text{B}_{12}\text{N}_{12}$ nanocage at a smaller adsorption distance (d_{ads}). Here these d_{ads} values are in the range of 1.61 (CH_3NH_2) to 3.12 Å (Cl_2) (Table 2). These findings are further validated by the adsorption energy of the gases on the $\text{B}_{12}\text{N}_{12}$ nanocage (see Table 2) and other structural changes (Table S1, ESI†). In all cases, the adsorption energy of the gases on the $\text{B}_{12}\text{N}_{12}$ nanocage is negative, suggesting that the

adsorption reaction is exothermic in nature. Typically, the gases strongly interact with the $\text{B}_{12}\text{N}_{12}$ nanocage at higher negative adsorption energies. Here these E_{ads} values are in the range of -0.83 (H_2) to -36.84 kcal mol^{-1} (CH_3NH_2). The E_{ads} values of the diatomic gases follow the order: $\text{H}_2 < \text{F}_2 < \text{N}_2 < \text{CO} < \text{Cl}_2 < \text{NO}$. The E_{ads} values of the triatomic molecules follow the order: $\text{OCS} < \text{CO}_2 < \text{N}_2\text{O} < \text{H}_2\text{Se} < \text{H}_2\text{S}$. The E_{ads} value of silane (-2.47 kcal mol^{-1}) is higher than that of methane (-1.70 kcal mol^{-1}). The E_{ads} values of the hydrocarbon gases follow the order: methane < acetylene < ethylene. The E_{ads} values of the halomethanes follow the order: $\text{CF}_4 < \text{CF}_2\text{Cl}_2 < \text{CHF}_3 < \text{CH}_3\text{Cl} < \text{CH}_3\text{F}$. The E_{ads} values of



Table 3 The reactivity indices, μ , η , S and ω for gas-adsorbed $B_{12}N_{12}$ nanocage. The values of μ , $\Delta\mu$, η , $\Delta\eta$, ω and $\Delta\omega$ are given in eV; the values of S and ΔS in (eV) $^{-1}$

Adsorbate	μ	$\Delta\mu$	η	$\Delta\eta$	S	ΔS	ω	$\Delta\omega$
SiH ₄	-4.72	0.01	4.71	-0.01	0.11	0.00	2.37	0.00
H ₂	-4.71	0.02	4.72	0.00	0.11	0.00	2.35	-0.02
Cl ₂	-5.99	-1.26	3.44	-1.28	0.15	0.04	5.22	2.85
F ₂	-5.45	-0.72	3.97	-0.75	0.13	0.02	3.75	1.38
CF ₄	-4.70	0.03	4.72	0.00	0.11	0.00	2.33	-0.04
CH ₄	-4.71	0.02	4.72	0.00	0.11	0.00	2.34	-0.03
CF ₂ Cl ₂	-4.66	0.07	4.72	0.00	0.11	0.00	2.31	-0.06
N ₂	-4.67	0.06	4.72	0.00	0.11	0.00	2.31	-0.06
CHF ₃	-4.71	0.02	4.71	-0.01	0.11	0.00	2.36	-0.01
OCS	-4.73	0.00	4.68	-0.04	0.11	0.00	2.39	0.02
N ₂ O	-4.70	0.03	4.71	-0.01	0.11	0.00	2.35	-0.02
AsH ₃	-4.17	0.56	4.66	-0.06	0.11	0.00	1.87	-0.50
CH ₃ Cl	-4.62	0.11	4.71	-0.01	0.11	0.00	2.27	-0.10
COCl ₂	-5.14	-0.41	4.14	-0.58	0.12	0.01	3.19	0.82
C ₂ H ₂	-4.60	0.13	4.70	-0.02	0.11	0.00	2.25	-0.12
C ₂ H ₄	-4.59	0.14	4.71	-0.01	0.11	0.00	2.23	-0.14
H ₂ Se	-4.45	0.28	4.49	-0.23	0.11	0.00	2.20	-0.17
H ₂ S	-4.29	0.44	4.64	-0.08	0.11	0.00	1.99	-0.38
PH ₃	-4.10	0.63	4.66	-0.06	0.11	0.00	1.80	-0.57
COF ₂	-4.57	0.16	4.71	-0.01	0.11	0.00	2.22	-0.15
CH ₃ F	-4.46	0.27	4.71	-0.01	0.11	0.00	2.11	-0.26
HCHO	-5.42	-0.69	3.25	-1.47	0.15	0.04	4.53	2.16
(CH ₃) ₂ O	-3.99	0.74	4.67	-0.05	0.11	0.00	1.70	-0.67
CH ₃ NH ₂	-4.00	0.73	4.57	-0.15	0.11	0.00	1.75	-0.62

formaldehyde and its halogenated derivatives follow the order: carbonyl fluoride < phosgene < formaldehyde. The E_{ads} value of dimethyl ether (-22.86 kcal mol $^{-1}$) is lower than that of both ammonia (-30.82 kcal mol $^{-1}$) and methylamine. The E_{ads} values of the pnictogen hydrides and methylamine follow the order arsine < phosphine < ammonia < methylamine. As shown in Fig. S3a (ESI †), these adsorption energies are found to be reasonably correlated with the adsorption distances (correlation coefficient of 0.742). Another important observation is that, as shown in Fig. 4a, these adsorption energies are well correlated with the MESP $V_{\text{min-X}}$ values of the gases (correlation coefficient of 0.9468). The angle of the hexagonal ring of the pristine $B_{12}N_{12}$ nanocage is 125° . This angle at the adsorption site decreases by at least 2° due to the adsorption of AsH₃, H₂Se, H₂S, PH₃, CH₃F, HCHO, (CH₃)₂O, and CH₃NH₂ (see Table S1, ESI †).

The entropic effects may also influence the adsorption processes. The analysis of G_{ads} values (Table 2) shows that the adsorption of most of the gases on the $B_{12}N_{12}$ nanocage is

endergonic, indicative of the weak interactions. However, the adsorption process is found to be exergonic for the HCHO/ $B_{12}N_{12}$, (CH₃)₂O/ $B_{12}N_{12}$, NH₃/ $B_{12}N_{12}$, and CH₃NH₂/ $B_{12}N_{12}$ systems. As shown in Fig. S4a (ESI †), these adsorption free energies are also well correlated with the MESP $V_{\text{min-X}}$ values of the gases (correlation coefficient of 0.9041).

The MESP maps of the gas-adsorbed $B_{12}N_{12}$ nanocage are given in Fig. 5. A visual check shows substantial changes in the MESP feature of the isolated molecules, mainly due to the strong gas adsorption. The blue color observed in the $B_{12}N_{12}$ nanocage is more marked in the presence of, for example, formaldehyde, dimethyl ether, and methylamine. The electronic changes associated with the adsorption process could be understood by comparing the MESP V_{min} of the isolated nanocage ($V_{\text{min-C}}$) with that of the gas-adsorbed nanocage (represented as $V_{\text{min-C'}}$) (see, e.g., Fig. S1, ESI †). We find that $\Delta V_{\text{min-C}} = V_{\text{min-C'}} - V_{\text{min-C}}$ is negative for all the studied systems (Table 2). This implies that the $B_{12}N_{12}$ nanocage becomes electron-rich due to the adsorption process. A large magnitude of $\Delta V_{\text{min-C}}$ has been observed, mainly due to the strong gas adsorption. Here these $\Delta V_{\text{min-C}}$ values are in the range of -0.50 (CH₄/ $B_{12}N_{12}$ system) to -14.50 kcal mol $^{-1}$ (CH₃NH₂/ $B_{12}N_{12}$ system).

The adsorption process could affect the HOMO and LUMO energies (see, e.g., Fig. S5, ESI †), and therefore, the DFT reactivity indices μ , η , S , and ω (see eqn (2)–(5)). The electrophilicity index ω consists of both the ability of the system to obtain additional electronic charge (driven by μ^2) and the resistance of the system to exchange electronic charge with the environment (driven by η). As a result, good electrophiles have higher (lower) values of $\mu(\eta)$. The DFT reactivity indices μ , η , S and ω of the $B_{12}N_{12}$ nanocage are -4.73 eV, 4.72 eV, 0.11 eV $^{-1}$ and 2.37 eV, respectively.²⁷ These DFT reactivity indices for the gas-adsorbed $B_{12}N_{12}$ nanocage are provided in Table 3. Substantial changes are found in these DFT reactivity indices, mainly due to the strong gas adsorption. The change in the reactivity index was calculated by taking the difference between the reactivity index of the gas-adsorbed nanocage and the reactivity index of the corresponding pristine nanocages. For example, the change in μ , $\Delta\mu$, and change in η , $\Delta\eta$, for the CH₄/ $B_{12}N_{12}$ system are 0.02 and 0.00 eV, respectively. The corresponding values for the CH₃NH₂/ $B_{12}N_{12}$ system are 0.73 and -0.15 eV respectively.

Table 4 The topological features, ρ_b , $\nabla^2\rho_b$, ELF, and LOL for the gas-adsorbed $B_{12}N_{12}$ nanocage. The values are given in a.u.

Adsorbate	ρ_b	$\nabla^2\rho_b$	ELF	LOL	Adsorbate	ρ_b	$\nabla^2\rho_b$	ELF	LOL
SiH ₄	0.010	0.027	0.051	0.189	CH ₃ Cl	0.016	0.041	0.077	0.225
H ₂	0.007	0.023	0.028	0.144	COCl ₂	0.018	0.056	0.059	0.201
Cl ₂	0.005	0.019	0.015	0.109	C ₂ H ₂	0.011	0.030	0.056	0.196
F ₂	0.007	0.029	0.012	0.098	C ₂ H ₄	0.013	0.030	0.079	0.226
CF ₄	0.012	0.041	0.032	0.153	H ₂ Se	0.049	-0.002	0.529	0.515
CH ₄	0.007	0.023	0.020	0.126	H ₂ S	0.064	-0.030	0.516	0.508
CF ₂ Cl ₂	0.012	0.043	0.033	0.155	PH ₃	0.089	-0.092	0.588	0.545
N ₂	0.011	0.037	0.034	0.159	COF ₂	0.018	0.056	0.062	0.204
CHF ₃	0.009	0.037	0.018	0.119	CH ₃ F	0.031	0.080	0.104	0.254
OCS	0.008	0.027	0.030	0.150	HCHO	0.090	0.336	0.129	0.278
N ₂ O	0.016	0.048	0.054	0.193	(CH ₃) ₂ O	0.102	0.410	0.139	0.287
AsH ₃	0.067	-0.053	0.683	0.595	CH ₃ NH ₂	0.125	0.314	0.219	0.346



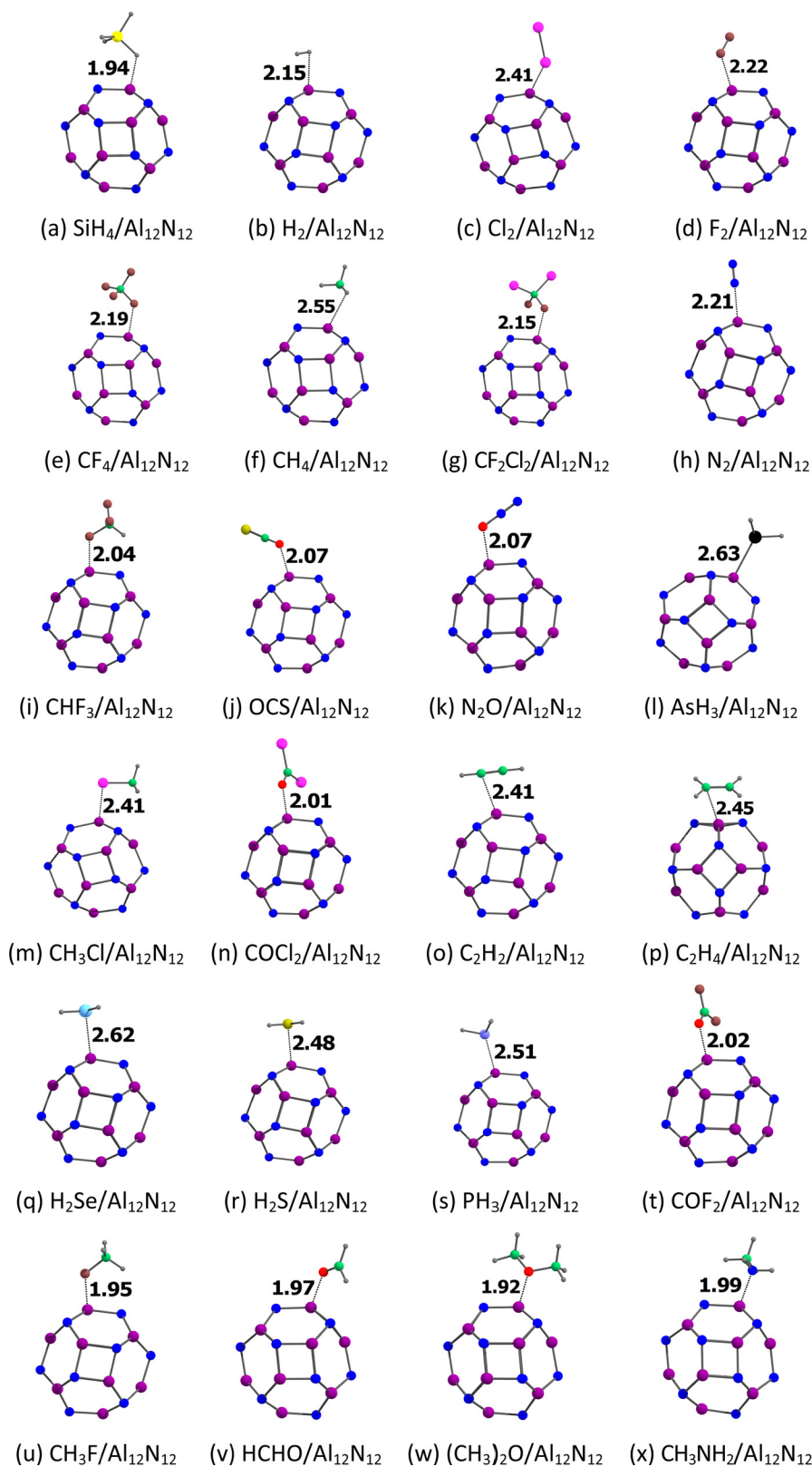


Fig. 6 Optimized structures of gases (a) SiH_4 , (b) H_2 , (c) Cl_2 , (d) F_2 , (e) CF_4 , (f) CH_4 , (g) CF_2Cl_2 , (h) N_2 , (i) CHF_3 , (j) OCS , (k) N_2O , (l) AsH_3 , (m) CH_3Cl , (n) COCl_2 , (o) C_2H_2 , (p) C_2H_4 , (q) H_2Se , (r) H_2S , (s) PH_3 , (t) COF_2 , (u) CH_3F , (v) HCHO , (w) $(\text{CH}_3)_2\text{O}$, and (x) CH_3NH_2 adsorbed on $\text{Al}_{12}\text{N}_{12}$. The adsorption distances are given in Å. The color code is the same as in Fig. 3. In addition, the Al atom is denoted by the purple color.



Table 5 Adsorption distance, E_{ads} , G_{ads} , MESP V_{min} , and ΔV_{min} for the gas-adsorbed $\text{Al}_{12}\text{N}_{12}$ nanocage. D_{ads} is given in Å, other values are given in kcal mol⁻¹

Adsorbate	d_{ads}	E_{ads}	G_{ads}	$V_{\text{min-C'}}$	$\Delta V_{\text{min-C}}$
SiH_4	1.94	-7.84	1.62	-57.17	-8.09
H_2	2.15	-3.66	3.75	-55.60	-6.53
Cl_2	2.41	-8.46	0.17	-53.59	-4.52
F_2	2.22	-3.59	3.82	-55.10	-6.02
CF_4	2.19	-4.54	5.11	-56.79	-7.72
CH_4	2.55	-4.65	1.52	-56.16	-7.09
CF_2Cl_2	2.15	-4.94	4.89	-57.92	-8.85
NO^a	2.22	-9.02	-0.40	-56.98	-7.91
N_2	2.21	-6.69	1.34	-57.10	-8.03
CHF_3	2.04	-10.94	-0.87	-57.42	-8.35
OCS	2.07	-9.50	-0.53	-60.37	-11.30
CO_2^a	2.08	-11.17	-2.52	-57.86	-8.79
N_2O	2.07	-12.93	-3.81	-59.11	-10.04
CO^a	2.20	-11.68	-3.04	-57.23	-8.16
AsH_3	2.63	-14.12	-4.29	-60.05	-10.98
CH_3Cl	2.41	-15.12	-4.48	-59.49	-10.42
COCl_2	2.01	-14.90	-3.94	-62.00	-12.93
C_2H_2	2.41	-14.35	-7.61	-58.17	-9.10
C_2H_4	2.45	-14.93	-4.51	-58.61	-9.54
H_2Se	2.62	-15.80	-6.29	-59.36	-10.29
H_2S	2.48	-16.74	-7.26	-59.30	-10.23
PH_3	2.51	-17.54	-8.03	-60.30	-11.23
COF_2	2.02	-14.81	-4.39	-60.74	-11.67
CH_3F	1.95	-17.72	-7.49	-60.74	-11.67
HCHO	1.97	-26.09	-14.15	-62.94	-13.87
$(\text{CH}_3)_2\text{O}$	1.92	-33.18	-21.28	-61.43	-12.36
NH_3^a	2.01	-36.83	-26.53	-62.12	-13.05
CH_3NH_2	1.99	-40.19	-28.68	-61.43	-12.36

^a Taken from ref. 27.

The results of the QTAIM analysis of the gas-adsorbed $\text{B}_{12}\text{N}_{12}$ nanocage are provided in Fig. S6 (ESI[†]) and Table 4. For the $\text{AsH}_3/\text{B}_{12}\text{N}_{12}$, $\text{H}_2\text{Se}/\text{B}_{12}\text{N}_{12}$, $\text{H}_2\text{S}/\text{B}_{12}\text{N}_{12}$, and $\text{PH}_3/\text{B}_{12}\text{N}_{12}$ systems, ρ_b values are in the range of 0.0491 ($\text{H}_2\text{Se}/\text{B}_{12}\text{N}_{12}$ system) to 0.0888 a.u. ($\text{PH}_3/\text{B}_{12}\text{N}_{12}$ system) and the corresponding $\nabla^2\rho_b$ values are negative. The QTAIM analysis suggests the covalent nature of interactions in these systems. For the rest of the systems, ρ_b values are in the range of 0.0051 ($\text{Cl}_2/\text{B}_{12}\text{N}_{12}$ system) to 0.1252 a.u. ($\text{CH}_3\text{NH}_2/\text{B}_{12}\text{N}_{12}$ system) and the corresponding $\nabla^2\rho_b$ values are positive. The QTAIM analysis suggests the noncovalent nature of interactions in these systems. For all the systems, the values of ELF and LOL are in the ranges of 0.012–0.683 and 0.098–0.595 a.u., respectively (see Table 4). The values of $\text{ELF} > 0.5$ and $\text{LOL} > 0.5$ in the $\text{AsH}_3/\text{B}_{12}\text{N}_{12}$, $\text{H}_2\text{Se}/\text{B}_{12}\text{N}_{12}$, $\text{H}_2\text{S}/\text{B}_{12}\text{N}_{12}$, and $\text{PH}_3/\text{B}_{12}\text{N}_{12}$ systems are also indicative of covalent interactions.

The NCI analysis provides the reduced density gradient (RDG) isosurface and the plots of the RDG versus $\text{sign}(\lambda_2)\rho$, where λ_2 is the second eigenvalue of the electron density Hessian matrix. The results of the NCI analysis of the gas-adsorbed $\text{B}_{12}\text{N}_{12}$ nanocage are provided in Fig. S7a and S8 (ESI[†]). The H-bond, van der Waals, and steric interactions can be visualized by blue, green, and red colors, respectively, in the NCI isosurface. Also, the H-bond ($\text{sign}(\lambda_2)\rho < 0$), van der Waals ($\text{sign}(\lambda_2)\rho \approx 0$), and steric ($\text{sign}(\lambda_2)\rho > 0$) interactions can be visualized as blue, green, and red colored spikes, respectively, in the RDG graph. The NCI results indicate the presence of

van der Waals interactions between the gas molecules and the $\text{B}_{12}\text{N}_{12}$ nanocage, except for the $\text{AsH}_3/\text{B}_{12}\text{N}_{12}$, $\text{H}_2\text{Se}/\text{B}_{12}\text{N}_{12}$, $\text{H}_2\text{S}/\text{B}_{12}\text{N}_{12}$, and $\text{PH}_3/\text{B}_{12}\text{N}_{12}$ systems. Overall, the steric interactions between the gas molecules and the $\text{B}_{12}\text{N}_{12}$ nanocage increases as the size of the gas molecules increases.

3.3. Adsorption of gases on $\text{Al}_{12}\text{N}_{12}$

The optimized structures of the gases adsorbed on the $\text{Al}_{12}\text{N}_{12}$ nanocage are given in Fig. 6. The studied gases are preferably bound to the Al atom rather than the N atom of the $\text{Al}_{12}\text{N}_{12}$ nanocage. Notably, the F atom of the CF_2Cl_2 , the O atom of the OCS , and the O atom of the N_2O are bound to the Al atom of the $\text{Al}_{12}\text{N}_{12}$ nanocage. Typically, the studied gases are strongly adsorbed on the $\text{Al}_{12}\text{N}_{12}$ nanocage. However, H_2 , F_2 , CF_4 , CH_4 , CF_2Cl_2 , and NO are weakly adsorbed on the $\text{Al}_{12}\text{N}_{12}$ nanocage. Typically, the gases strongly interact with the $\text{Al}_{12}\text{N}_{12}$ nanocage at a smaller adsorption distance (d_{ads}). Here these d_{ads} values are in the range of 1.92 ($(\text{CH}_3)_2\text{O}$) to 2.63 Å (AsH_3) (Table 5). These findings are further validated by the adsorption energy of the gases on the $\text{Al}_{12}\text{N}_{12}$ nanocage (see Table 5) and other structure changes (Table S2, ESI[†]). In all cases, the adsorption energy of the gases on the $\text{Al}_{12}\text{N}_{12}$ nanocage is negative, suggesting that the adsorption reaction is exothermic in nature. Typically, the gases strongly interact with the $\text{Al}_{12}\text{N}_{12}$ nanocage at higher negative adsorption energies. Here these E_{ads} values are in the range of -3.59 (F_2) to -40.19 kcal mol⁻¹ (CH_3NH_2). The E_{ads} values of the diatomic gases follow the order: $\text{F}_2 < \text{H}_2 < \text{N}_2 < \text{Cl}_2 < \text{NO} < \text{CO}$. The E_{ads} values of the triatomic molecules follow the order: $\text{OCS} < \text{CO}_2 < \text{N}_2\text{O} < \text{H}_2\text{Se} < \text{H}_2\text{S}$. The E_{ads} value of silane (-7.84 kcal mol⁻¹) is higher than that of methane (-4.65 kcal mol⁻¹). The E_{ads} values of the hydrocarbon gases follow the order: methane < acetylene < ethylene. The E_{ads} values of the halomethanes follow the order: $\text{CF}_4 < \text{CF}_2\text{Cl}_2 < \text{CHF}_3 < \text{CH}_3\text{Cl} < \text{CH}_3\text{F}$. The E_{ads} values of formaldehyde and its halogenated derivatives follow the order: carbonyl fluoride < phosgene < formaldehyde. The E_{ads} value of dimethyl ether (-33.18 kcal mol⁻¹) is lower than that of both ammonia (-36.83 kcal mol⁻¹) and methylamine. The E_{ads} values of the pnictogen hydrides and methylamine follow the order arsine < phosphine < ammonia < methylamine. As shown in Fig. S3b (ESI[†]), these adsorption energies are not well correlated with the adsorption distances (correlation coefficient of 0.293). Another important observation is that, as shown in Fig. 4b, these adsorption energies are well correlated with the MESP $V_{\text{min-X}}$ values of the gases (correlation coefficient of 0.9808). The angle of the hexagonal ring of the pristine $\text{Al}_{12}\text{N}_{12}$ nanocage is 125°. This angle at the adsorption site is almost unaffected by the adsorption of H_2 , F_2 , CF_4 , CH_4 , and CF_2Cl_2 (see Table S2, ESI[†]).

The analysis of G_{ads} values (Table 5) shows that the adsorption of most of the gases on the $\text{Al}_{12}\text{N}_{12}$ nanocage is exergonic, indicative of the stronger interactions. However, the adsorption process is found to be endergonic for the $\text{SiH}_4/\text{Al}_{12}\text{N}_{12}$, $\text{H}_2/\text{Al}_{12}\text{N}_{12}$, $\text{Cl}_2/\text{Al}_{12}\text{N}_{12}$, $\text{F}_2/\text{Al}_{12}\text{N}_{12}$, $\text{CF}_4/\text{Al}_{12}\text{N}_{12}$, $\text{CH}_4/\text{Al}_{12}\text{N}_{12}$, $\text{CF}_2\text{Cl}_2/\text{Al}_{12}\text{N}_{12}$, and $\text{N}_2/\text{Al}_{12}\text{N}_{12}$ systems. As shown in Fig. S4b (ESI[†]), these adsorption free energies are also well correlated



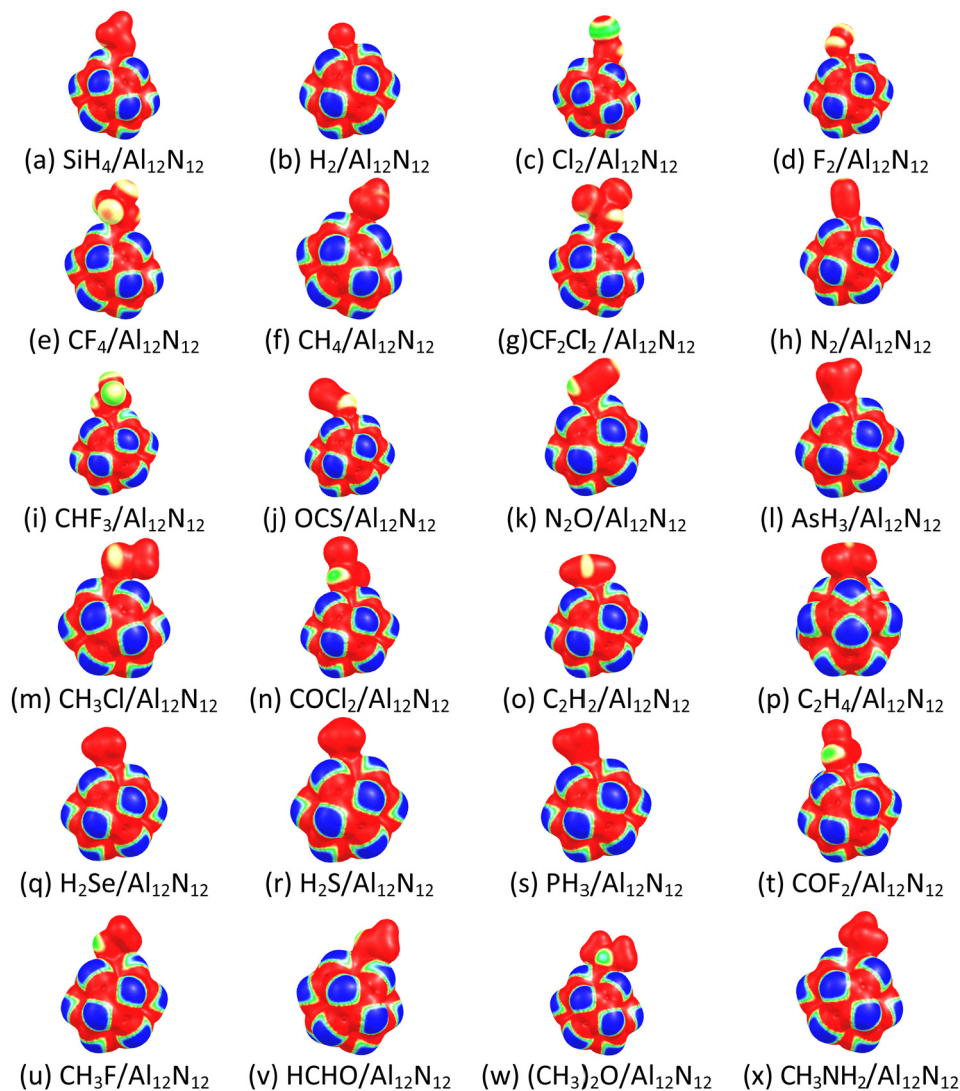


Fig. 7 MESP mapped onto 0.01 a.u. electron density isosurface of gases (a) SiH₄, (b) H₂, (c) Cl₂, (d) F₂, (e) CF₄, (f) CH₄, (g) CF₂Cl₂, (h) N₂, (i) CHF₃, (j) OCS, (k) N₂O, (l) AsH₃, (m) CH₃Cl, (n) COCl₂, (o) C₂H₂, (p) C₂H₄, (q) H₂Se, (r) H₂S, (s) PH₃, (t) COF₂, (u) CH₃F, (v) HCHO, (w) (CH₃)₂O, and (x) CH₃NH₂ adsorbed on Al₁₂N₁₂. The color code is the same as in Fig. 2.

with the MESP $V_{\min-x}$ values of the gases (correlation coefficient of 0.9818).

The MESP maps of the gas-adsorbed Al₁₂N₁₂ nanocage are given in Fig. 7. A visual check shows substantial changes in the MESP feature of most of the isolated gas molecules due to the adsorption process. The blue region (most electron-rich region) in, for example, the formaldehyde, dimethyl ether, and methylamine molecules is less marked in the presence of Al₁₂N₁₂. We find that $\Delta V_{\min-C}$ is negative for all the studied systems (Table 5). This implies that the Al₁₂N₁₂ nanocage becomes electron-rich due to the adsorption process. Here in most of the systems, a large magnitude of $\Delta V_{\min-C}$ has been observed due to the adsorption process. These $\Delta V_{\min-C}$ values are in the range of -4.52 (Cl₂/Al₁₂N₁₂ system) to -13.87 kcal mol⁻¹ (HCHO/Al₁₂N₁₂ system).

The DFT reactivity indices μ , η , S and ω of the Al₁₂N₁₂ nanocage are -4.86 eV, 3.16 eV, 0.16 eV⁻¹ and 3.74 eV,

respectively.²⁷ In most of the systems, substantial changes are observed in these DFT reactivity indices due to the adsorption process (Table 6). For example, $\Delta\mu$ and $\Delta\eta$ for the CH₄/Al₁₂N₁₂ system are 0.11 and 0.00 eV, respectively. The corresponding values for the CH₃NH₂/Al₁₂N₁₂ system are 0.43 and -0.03 eV respectively.

The results of the QTAIM analysis of the gas-adsorbed Al₁₂N₁₂ nanocage are provided in Fig. S9 (ESI[†]) and Table 7. For all the systems, ρ_b values are in the range of 0.0122 (CH₄/Al₁₂N₁₂ system) to 0.0587 a.u. (CH₃NH₂/Al₁₂N₁₂ system) and the corresponding $\nabla^2\rho_b$ values are positive. For all the systems, the values of ELF and LOL are in the ranges of 0.030 – 0.214 and 0.150 – 0.343 a.u., respectively (see Table 7). These results suggest the noncovalent nature of interactions in these systems. The results of the NCI analysis of the gas-adsorbed Al₁₂N₁₂ nanocage are provided in Fig. S7b and S10 (ESI[†]). The NCI results indicate the presence of van der Waals interactions



Table 6 The reactivity indices, μ , η , S and ω for the gas-adsorbed $\text{Al}_{12}\text{N}_{12}$ nanocage. The values of μ , $\Delta\mu$, η , $\Delta\eta$, ω and $\Delta\omega$ are given in eV; the values of S and ΔS in $(\text{eV})^{-1}$

Adsorbate	μ	$\Delta\mu$	η	$\Delta\eta$	S	ΔS	ω	$\Delta\omega$
SiH_4	-4.69	0.17	3.16	0.00	0.16	0.00	3.49	-0.25
H_2	-4.75	0.11	3.18	0.02	0.16	0.00	3.54	-0.20
Cl_2	-5.32	-0.46	2.80	-0.36	0.18	0.02	5.06	1.32
F_2	-5.44	-0.58	2.52	-0.64	0.20	0.04	5.87	2.13
CF_4	-4.71	0.15	3.18	0.02	0.16	0.00	3.50	-0.24
CH_4	-4.75	0.11	3.16	0.00	0.16	0.00	3.57	-0.17
CF_2Cl_2	-4.66	0.20	3.17	0.01	0.16	0.00	3.43	-0.31
N_2	-4.68	0.18	3.19	0.03	0.16	0.00	3.44	-0.30
CHF_3	-4.71	0.15	3.16	0.00	0.16	0.00	3.52	-0.22
OCS	-4.59	0.27	3.15	-0.01	0.16	0.00	3.33	-0.41
N_2O	-4.63	0.23	3.15	-0.01	0.16	0.00	3.40	-0.34
AsH_3	-4.52	0.34	3.16	0.00	0.16	0.00	3.24	-0.50
CH_3Cl	-4.60	0.26	3.16	0.00	0.16	0.00	3.34	-0.40
COCl_2	-4.93	-0.07	2.74	-0.42	0.18	0.02	4.43	0.69
C_2H_2	-4.59	0.27	3.16	0.00	0.16	0.00	3.33	-0.41
C_2H_4	-4.60	0.26	3.15	-0.01	0.16	0.00	3.35	-0.39
H_2Se	-4.56	0.30	3.16	0.00	0.16	0.00	3.29	-0.45
H_2S	-4.58	0.28	3.16	0.00	0.16	0.00	3.32	-0.42
PH_3	-4.51	0.35	3.16	0.00	0.16	0.00	3.21	-0.53
COF_2	-4.56	0.30	3.17	0.01	0.16	0.00	3.29	-0.45
CH_3F	-4.53	0.33	3.14	-0.02	0.16	0.00	3.27	-0.47
HCHO	-4.75	0.11	2.87	-0.29	0.17	0.01	3.93	0.19
$(\text{CH}_3)_2\text{O}$	-4.45	0.41	3.14	-0.02	0.16	0.00	3.16	-0.58
CH_3NH_2	-4.43	0.43	3.13	-0.03	0.16	0.00	3.13	-0.61

between the gas molecules and the $\text{Al}_{12}\text{N}_{12}$ nanocage. Overall, the steric interactions between the gas molecules and the $\text{Al}_{12}\text{N}_{12}$ nanocage increase as the size of the gas molecules increases.

Our results show that only AsH_3 , H_2Se , H_2S , PH_3 , CH_3F , HCHO , $(\text{CH}_3)_2\text{O}$, and CH_3NH_2 are strongly adsorbed on the $\text{B}_{12}\text{N}_{12}$ nanocage. Furthermore, only H_2 , F_2 , CF_4 , CH_4 , and CF_2Cl_2 are weakly adsorbed on the $\text{Al}_{12}\text{N}_{12}$ nanocage. Overall, our results indicate that the $\text{Al}_{12}\text{N}_{12}$ nanoclusters may have a higher potential in gas storage and catalytic applications than the $\text{B}_{12}\text{N}_{12}$ nanoclusters. The stronger the adsorption of gas molecules, the more difficult it is for them to desorb from the surface.⁷⁸ The gas-sensing behavior of the $\text{Al}_{12}\text{N}_{12}$ nanocage might have a severe influence on the reusability of gas sensors. The MESP of a molecule is a real physical property that can be determined experimentally by X-ray diffraction techniques or by computational methods.⁵⁸ There is a strong linear correlation between the adsorption energies of the gas-adsorbed $\text{B}_{12}\text{N}_{12}$ and $\text{Al}_{12}\text{N}_{12}$ systems and the MESP V_{\min} values

of the gases (see Fig. 4). This enables us to predict the adsorption energies once we know the MESP features of the gas molecules.

4. Conclusions

The adsorption of twenty-four gases (SiH_4 , H_2 , Cl_2 , F_2 , CF_4 , CH_4 , CF_2Cl_2 , N_2 , CHF_3 , OCS , N_2O , AsH_3 , CH_3Cl , COCl_2 , C_2H_2 , C_2H_4 , H_2Se , H_2S , PH_3 , COF_2 , CH_3F , HCHO , $(\text{CH}_3)_2\text{O}$, and CH_3NH_2) on the $\text{B}_{12}\text{N}_{12}$ and $\text{Al}_{12}\text{N}_{12}$ nanocages was studied using DFT calculations. Most of the studied gases are weakly adsorbed on the $\text{B}_{12}\text{N}_{12}$ nanocage. However, AsH_3 , H_2Se , H_2S , PH_3 , CH_3F , HCHO , $(\text{CH}_3)_2\text{O}$, and CH_3NH_2 are strongly adsorbed on the $\text{B}_{12}\text{N}_{12}$ nanocage. The gases strongly interact with the nanocage usually at a smaller adsorption distance and a higher negative adsorption energy. For the gas-adsorbed $\text{B}_{12}\text{N}_{12}$ system, the d_{ads} values are in the range of 1.61 (CH_3NH_2) to 3.12 Å (Cl_2), and the E_{ads} values are in the range of -0.83 (H_2) to -36.84 kcal mol⁻¹ (CH_3NH_2). Here the adsorption energies are found to be reasonably correlated with the adsorption distances. Another important observation is that these adsorption energies are well correlated with the MESP V_{\min} values of the gases. Substantial changes are found in the DFT reactivity indices (μ , η , S and ω) of the $\text{B}_{12}\text{N}_{12}$ nanocage, mainly due to the strong gas adsorption. For example, $\Delta\mu$ and $\Delta\eta$ for the $\text{CH}_4/\text{B}_{12}\text{N}_{12}$ system are 0.02 and 0.00 eV, respectively. The corresponding values for the $\text{CH}_3\text{NH}_2/\text{B}_{12}\text{N}_{12}$ system are 0.73 and -0.15 eV respectively. The QTAIM analysis suggests the covalent nature of interactions in the $\text{AsH}_3/\text{B}_{12}\text{N}_{12}$, $\text{H}_2\text{Se}/\text{B}_{12}\text{N}_{12}$, $\text{H}_2\text{S}/\text{B}_{12}\text{N}_{12}$, and $\text{PH}_3/\text{B}_{12}\text{N}_{12}$ systems.

Most of the studied gases are strongly adsorbed on the $\text{Al}_{12}\text{N}_{12}$ nanocage. However, H_2 , F_2 , CF_4 , CH_4 , and CF_2Cl_2 are weakly adsorbed on the $\text{Al}_{12}\text{N}_{12}$ nanocage. For the gas-adsorbed $\text{Al}_{12}\text{N}_{12}$ system, the d_{ads} values are in the range of 1.92 ($(\text{CH}_3)_2\text{O}$) to 2.63 Å (AsH_3), and the E_{ads} values are in the range of -3.59 (F_2) to -40.19 kcal mol⁻¹ (CH_3NH_2). These adsorption energies are also well correlated with the MESP $V_{\min-X}$ values of the gases. In most of the systems, substantial changes are observed in the DFT reactivity indices (μ , η , S and ω) of the $\text{Al}_{12}\text{N}_{12}$ nanocage due to the gas adsorption. For example, $\Delta\mu$ and $\Delta\eta$ for the $\text{CH}_4/\text{Al}_{12}\text{N}_{12}$ system are 0.11 and 0.00 eV, respectively. The corresponding values for the $\text{CH}_3\text{NH}_2/\text{Al}_{12}\text{N}_{12}$ system are 0.43 and -0.03 eV

Table 7 The topological features, ρ_b , $\nabla^2\rho_b$, ELF, and LOL for the gas-adsorbed $\text{Al}_{12}\text{N}_{12}$ nanocage. The values are given in a.u.

Adsorbate	ρ_b	$\nabla^2\rho_b$	ELF	LOL	Adsorbate	ρ_b	$\nabla^2\rho_b$	ELF	LOL
SiH_4	0.028	0.082	0.085	0.234	CH_3Cl	0.040	0.165	0.081	0.229
H_2	0.020	0.063	0.058	0.198	COCl_2	0.042	0.276	0.048	0.184
Cl_2	0.048	0.134	0.214	0.343	C_2H_2	0.029	0.085	0.093	0.243
F_2	0.021	0.100	0.034	0.157	C_2H_4	0.029	0.069	0.116	0.266
CF_4	0.022	0.118	0.030	0.150	H_2Se	0.032	0.082	0.111	0.261
CH_4	0.012	0.034	0.068	0.213	H_2S	0.035	0.103	0.104	0.254
CF_2Cl_2	0.024	0.137	0.030	0.151	PH_3	0.038	0.096	0.125	0.275
N_2	0.028	0.148	0.042	0.173	COF_2	0.040	0.258	0.048	0.184
CHF_3	0.032	0.208	0.037	0.164	CH_3F	0.041	0.294	0.042	0.173
OCS	0.034	0.208	0.095	0.245	HCHO	0.049	0.325	0.059	0.200
N_2O	0.036	0.212	0.047	0.183	$(\text{CH}_3)_2\text{O}$	0.056	0.395	0.060	0.201
AsH_3	0.033	0.072	0.128	0.277	CH_3NH_2	0.059	0.335	0.082	0.230



respectively. The QTAIM analysis suggests the noncovalent nature of interactions in the gas-adsorbed $\text{Al}_{12}\text{N}_{12}$ systems.

Conflicts of interest

There are no conflicts to declare.

Acknowledgements

This publication is based upon work supported by the King Abdullah University of Science and Technology (KAUST) Office of Sponsored Research (OSR) under award no. ORFS-2022-CRG11-5028. R. G. S. N. and A. K. N. N. would like to thank KAUST for providing the computational resources of the Shaheen II supercomputer.

References

- 1 U.S. EPA's report global mitigation of non- CO_2 greenhouse gases: 2010–2030.
- 2 H. Tian, *et al.*, *Nature*, 2020, **586**, 248–256.
- 3 J. F. d S. Petrucci and A. A. Cardoso, *Anal. Chem.*, 2016, **88**, 11714–11719.
- 4 P. D. N. Svoronos and T. J. Bruno, *Ind. Eng. Chem. Res.*, 2002, **41**, 5321–5336.
- 5 G. W. Gribble, *J. Nat. Prod.*, 1992, **55**, 1353–1395.
- 6 F. S. Rowland, *Am. Sci.*, 1989, **77**, 36–45.
- 7 J.-R. Chen, H.-Y. Tsai, S.-K. Chen, H.-R. Pan, S.-C. Hu, C.-C. Shen, C.-M. Kuan, Y.-C. Lee and C.-C. Wu, *Proc. Safety Prog.*, 2006, **25**, 237–244.
- 8 Y. N. Ko, S. H. Choi and Y. C. Kang, *ACS Appl. Mater. Interfaces*, 2016, **8**, 6449–6456.
- 9 C. Winder, *Environ. Res.*, 2001, **85**, 105–114.
- 10 J. Wang, M. Sánchez-Roselló, J. L. Aceña, C. del Pozo, A. E. Sorochinsky, S. Fustero, V. A. Soloshonok and H. Liu, *Chem. Rev.*, 2014, **114**, 2432–2506.
- 11 D. L. Sudakin, *Hum. Exp. Toxicol.*, 2005, **24**, 27–33.
- 12 D. Pakulska and S. Czerczak, *Int. J. Occup. Med. Environ. Health*, 2006, **19**, 36–44.
- 13 J. Borak and W. F. Diller, *J. Occup. Environ. Med.*, 2001, **43**, 110–119.
- 14 Y. Mitsui, Y. Ohira, T. Yonemura, T. Takaichi, A. Sekiya and T. Beppu, *J. Electrochem. Soc.*, 2004, **151**, G297.
- 15 T. Salthammer, S. Mentese and R. Marutzky, *Chem. Rev.*, 2010, **110**, 2536–2572.
- 16 T. H. Fleisch, A. Basu, M. J. Gradassi and J. G. Masin, *Stud. Surf. Sci. Catal.*, 1997, **107**, 117–125.
- 17 S. R. Raga, Y. Jiang, L. K. Ono and Y. Qi, *Energy Technol.*, 2017, **5**, 1750–1761.
- 18 D. Mori and K. Hirose, *Int. J. Hydrogen Energy*, 2009, **34**, 4569–4574.
- 19 C. Nguyen and D. D. Do, *Langmuir*, 1999, **15**, 3608–3615.
- 20 V. K. Gupta and T. A. Saleh, *Environ. Sci. Pollut. Res. Int.*, 2013, **20**, 2828–2843.
- 21 S. Gadipelli and Z. X. Guo, *Prog. Mater. Sci.*, 2015, **69**, 1–60.
- 22 N. Rangnekar, N. Mittal, B. Elyassi, J. Caro and M. Tsapatsis, *Chem. Soc. Rev.*, 2015, **44**, 7128–7154.
- 23 Y. Yang, A. K. Narayanan Nair and S. Sun, *J. Phys. Chem. C*, 2020, **124**, 16478–16487.
- 24 Y. Yang, A. K. Narayanan Nair and S. Sun, *Ind. Eng. Chem. Res.*, 2021, **60**, 7729–7738.
- 25 A. K. Narayanan Nair, R. Cui and S. Sun, *ACS Earth Space Chem.*, 2021, **5**, 2599–2611.
- 26 R. Geetha Sadasivan Nair, A. Kumar Narayanan Nair and S. Sun, *J. Mol. Liq.*, 2023, 122923.
- 27 R. Geetha Sadasivan Nair, A. K. Narayanan Nair and S. Sun, *Energy Fuels*, 2023, **37**, 14053–14063.
- 28 A. Abbasi and J. Jahanbin Sardroodi, *Environ. Sci.: Nano*, 2016, **3**, 1153–1164.
- 29 A. Abbasi, J. J. Sardroodi and A. R. Ebrahimzadeh, *Surf. Sci.*, 2016, **654**, 20–32.
- 30 A. Abbasi and J. J. Sardroodi, *Surf. Interfaces*, 2017, **8**, 15–27.
- 31 A. Abbasi and J. Jahanbin Sardroodi, *New J. Chem.*, 2017, **41**, 12569–12580.
- 32 A. Abbasi and J. J. Sardroodi, *J. Nanostruct. Chem.*, 2017, **7**, 345–358.
- 33 C. Zhao and H. Wu, *Appl. Surf. Sci.*, 2018, **435**, 1199–1212.
- 34 A. Abbasi and J. J. Sardroodi, *Comput. Theor. Chem.*, 2018, **1125**, 15–28.
- 35 A. Abbasi and J. J. Sardroodi, *Phys. E*, 2019, **108**, 382–390.
- 36 A. Abbasi and J. J. Sardroodi, *Appl. Surf. Sci.*, 2019, **469**, 781–791.
- 37 A. Abbasi, A. Abdelrasoul and J. J. Sardroodi, *Adsorption*, 2019, **25**, 1001–1017.
- 38 J. Beheshtian, A. A. Peyghan, Z. Bagheri and M. Kamfiroozi, *Struct. Chem.*, 2012, **23**, 1567–1572.
- 39 K. Kalateh and A. Abdolmanafi, *Int. J. New Chem.*, 2015, **2**, 1–7.
- 40 E. Shakerzadeh, *Phys. E*, 2016, **78**, 1–9.
- 41 A. Bahrami, M. B. Qarai and N. L. Hadipour, *Comput. Theor. Chem.*, 2017, **1108**, 63–69.
- 42 A. S. Rad, *Semiconductors*, 2017, **51**, 134–138.
- 43 S. Larki, E. Shakerzadeh, E. C. Anot and R. Behjatmanesh-Ardakani, *Chem. Phys.*, 2019, **526**, 110424.
- 44 A. Shokuhi Rad, D. Zareyee, V. Pouralijan Foukolaei, B. Kamyab Moghadas and M. Peyravi, *Mol. Phys.*, 2016, **114**, 3143–3149.
- 45 L. Saedi, Z. Javanshir, S. Khanahmadzadeh, M. Maskanati and M. Nouraliei, *Mol. Phys.*, 2020, **118**, e1658909.
- 46 A. S. Rad and K. Ayub, *Mater. Chem. Phys.*, 2017, **194**, 337–344.
- 47 M. Y. Mehboob, R. Hussain, F. Younas, S. Jamil, M. M. A. Iqbal, K. Ayub, N. Sultana and M. R. S. A. Janjua, *J. Clust. Sci.*, 2023, **34**, 1237–1247.
- 48 A. S. Rad and K. Ayub, *Vacuum*, 2016, **133**, 70–80.
- 49 Q. Wang, Q. Sun, P. Jena and Y. Kawazoe, *ACS Nano*, 2009, **3**, 621–626.
- 50 A. S. Rad, *J. Theory Comput. Chem.*, 2018, **17**, 1850013.
- 51 R. Padash, M. Rahimi-Nasrabadi, A. Shokuhi Rad, A. Sobhani-Nasab, T. Jesionowski and H. Ehrlich, *J. Clust. Sci.*, 2019, **30**, 203–218.



- 52 T. Oku, A. Nishiwaki and I. Narita, *Sci. Technol. Adv.*, 2004, **5**, 635–638.
- 53 C. Balasubramanian, S. Bellucci, P. Castrucci, M. De Crescenzi and S. V. Bhorkaskar, *Chem. Phys. Lett.*, 2004, **383**, 188–191.
- 54 C. Liu, Z. Hu, Q. Wu, X. Wang, Y. Chen, H. Sang, J. Zhu, S. Deng and N. Xu, *J. Am. Chem. Soc.*, 2005, **127**, 1318–1322.
- 55 H.-S. Wu, F.-Q. Zhang, X.-H. Xu, C.-J. Zhang and H. Jiao, *J. Phys. Chem. A*, 2003, **107**, 204–209.
- 56 G. S. Remya and C. H. Suresh, *New J. Chem.*, 2018, **42**, 3602–3608.
- 57 G. S. Remya and C. H. Suresh, *New J. Chem.*, 2019, **43**, 14634–14642.
- 58 C. H. Suresh, G. S. Remya and P. K. Anjalikrishna, *Wiley Interdiscip. Rev.: Comput. Mol. Sci.*, 2022, **12**, e1601.
- 59 M. J. Frisch, *et al.*, *Gaussian 16, Revision A.03*, Gaussian, Inc., Wallingford, CT, 2016.
- 60 Y. Zhao and D. G. Truhlar, *Theor. Chem. Acc.*, 2008, **120**, 215–241.
- 61 H. Chermette, *J. Comput. Chem.*, 1999, **20**, 129–154.
- 62 R. G. Parr, R. A. Donnelly, M. Levy and W. E. Palke, *J. Chem. Phys.*, 1978, **68**, 3801–3807.
- 63 L. R. Domingo, M. Ríos-Gutiérrez and P. Pérez, *Molecules*, 2016, **21**, 748.
- 64 P. K. Chattaraj, U. Sarkar and D. R. Roy, *Chem. Rev.*, 2006, **106**, 2065–2091.
- 65 R. G. Parr and R. G. Pearson, *J. Am. Chem. Soc.*, 1983, **105**, 7512–7516.
- 66 R. G. Parr, L. v Szentpály and S. Liu, *J. Am. Chem. Soc.*, 1999, **121**, 1922–1924.
- 67 S. F. Boys and F. Bernardi, *Mol. Phys.*, 1970, **19**, 553–566.
- 68 R. F. Bader, *Chem. Rev.*, 1991, **91**, 893–928.
- 69 T. Lu and F. Chen, *J. Comput. Chem.*, 2012, **33**, 580–592.
- 70 P. A. Hunt, C. R. Ashworth and R. P. Matthews, *Chem. Soc. Rev.*, 2015, **44**, 1257–1288.
- 71 S. Khan, H. Sajid, K. Ayub and T. Mahmood, *J. Mol. Liq.*, 2020, **316**, 113860.
- 72 A. Savin, R. Nesper, S. Wengert and T. F. Fässler, *Angew. Chem., Int. Ed. Engl.*, 1997, **36**, 1808–1832.
- 73 A. V. Afonin, V. A. Semenov and A. V. Vashchenko, *Phys. Chem. Chem. Phys.*, 2021, **23**, 24536–24540.
- 74 E. R. Johnson, S. Keinan, P. Mori-Sánchez, J. Contreras-García, A. J. Cohen and W. Yang, *J. Am. Chem. Soc.*, 2010, **132**, 6498–6506.
- 75 J. Contreras-García, E. R. Johnson, S. Keinan, R. Chaudret, J. P. Piquemal, D. N. Beratan and W. Yang, *J. Chem. Theory Comput.*, 2011, **7**, 625–632.
- 76 T. Williams and C. Kelley, *GNUplot: an interactive plotting program*, 1998.
- 77 W. Humphrey, A. Dalke and K. Schulten, *J. Mol. Graph.*, 1996, **14**, 33–38.
- 78 A. L. Pereira Silva and J. d J. G. Varela Júnior, *Inorg. Chem.*, 2023, **62**, 1926–1934.

